Analysis of actively-confined concrete columns using prestressed steel tubes

Mahdi Nematzadeh[*] and Akbar Haghinejad

Department of Civil Engineering, University of Mazandaran, Babolsar, Iran

Abstract. In this paper, an innovative technique for finite element (FE) modeling of steel tube-confined concrete (STCC) columns with active confinement under axial compressive loading is presented. In this method, a new constitutive model for the stress-strain relationship of actively-confined concrete is proposed. In total, 14 series of experimental STCC stub columns having active confinement were modeled using the ABAQUS software. The results obtained from the 3D model including the compressive strength at the initial peak point and failure point, as well as the axial and lateral stress-strain curves were compared with the experimental results to verify the accuracy of the 3D model. It was found that there existed a good agreement between them. A parametric study was conducted to investigate the effect of the concrete compressive strength, steel tube wall thickness, and pre-stressing level on the behavior of STCC columns with active confinement. The results indicated that increasing the concrete core's compressive strength leads to an increase in the compressive strength of the active composite column as well as its earlier failure. Furthermore, a reduction in the tube external diameter-to-wall thickness ratio affects the axial stress-strain curve and the confining pressure, while increasing the pre-stressing level has a negligible effect on the two.

Keywords: concrete constitutive models; confined concrete; finite elements method; pre-tensioned concrete; computer modeling

1. Introduction

Steel tube-confined concrete (STCC) columns are increasingly employed in many structural applications such as high-rise buildings and bridge piers. In this type of composite column, the loading is applied only to the concrete core; hence, the STCC columns are employed in concrete structures in which the steel tube is cut near the beam-column joint. Steel members have several advantages such as high tensile strength and ductility, while high compressive strength and stiffness are among concrete members' characteristics. The composite action of the concrete core and steel tube leads to better properties of these columns compared with those of plain concrete and steel columns. In STCC columns, the steel tube has more of a confining role than an axial load-bearing role, resulting in an increase in the strength and ductility of the column relative to those of the conventional reinforced concrete column via the prevention of lateral dilation of the concrete member. In addition, the likelihood of local buckling of the steel tube decreases as a result of a small axial load carried by the steel tube as well as the concrete infill. Moreover, the steel tubes in composite columns serve as permanent formworks, which results in the reduction of the construction cost and time.

Extensive analytical research has been carried out to predict the behavior of composite columns (Yu *et al.* 2010, Gupta *et al.* 2015, Shraideh and Aboutaha 2013). Using the experimental results of Han *et al.* (2005), Yu *et al.* (2010)

presented a finite element model by means of the ABAQUS program, thereby investigated the behavior of STCC columns, and then, compared the obtained results with those of concrete-filled steel tube (CFST) columns. Wang *et al.* (2011) performed a numerical study on the behavior of STCC columns as a part of their research and indicated a high confinement for the concrete core as well as a low likelihood for the local buckling of the steel tube as a result of the small load carried by it. Employing the ABAQUS finite element program, Schneider (1998) developed a model to determine the behavior of CFST columns, in which the unconfined concrete stress-strain curve is used for the definition of the concrete properties. The proposed model predicted the elastic and inelastic behavior of the columns with high accuracy. Hu *et al.* (2003) utilized the confined concrete stress-strain curve and the steel bilinear stress-strain curve to define the properties of concrete and steel, respectively, in ABAQUS. The finite element analysis results were verified with respect to the experimental results of Schneider (1998) and Huang *et al.* (2002), and then, via trial and error, equations were developed for determining the confining pressure. Ellobody *et al.* (2006) utilized the confined concrete stress-strain curve and the steel multi-linear stress-strain curve to define the behavior of concrete and steel materials, respectively, in the ABAQUS. They studied the effect of concrete strength and cross section dimensions on the compressive behavior of CFST columns in a parametric study. Johansson and Gylltoft (2002) investigated the mechanical behavior of steel-concrete composite columns under various loading conditions in experimental and analytical investigations, and developed a 3D finite element model which was then verified with respect to the experimental results and subsequently

---

*Corresponding author, Assistant Professor
E-mail: m.nematzadeh@umz.ac.ir

employed to study the mechanical behavior of a column experiencing the interaction between the concrete core and steel tube. In their previous study, Haghinejad and Nematzadeh (2016) proposed a 3D finite element model using the ABAQUS software to predict the behavior of STCC columns with passive confinement. They proposed new values for the passive confinement parameters through calibration and matching the results obtained from the finite element analysis (FEA) with those of the experiments conducted by Nematzadeh *et al.* (2017a) for the STCC columns.

Generally, confinement is applied to the concrete core either passively or actively. In the passive type, the concrete core needs to undergo a significant lateral deformation to experience an effective confinement by the confining member, which leads to a reduction in the effect of confinement on improving the compressive properties of the composite section. One way to avoid large lateral deformation of concrete is the use of methods to create active confinement. In active confinement, the concrete core is under lateral pressure before loading. The presence of lateral pressure delays concrete cracking under axial compressive load, thus a better compressive behavior is obtained for the concrete. There are various experimental methods for pre-stressing the confining member and producing active confinement in the composite columns. Use of expansive materials in the concrete mixture (Chang *et al.* 2009, Mortazavi *et al.* 2003), as well as pre-stressing the transverse hoops (Shinohara 2008) are among the methods employed for lateral pre-tensioning. Pre-stressing continuous spirals (Feeser and Chinn 1962, Janke *et al.* 2009) or individual strips (Moghaddam *et al.* 2010), and thermal pre-stressing of steel confining components (Mokari and Moghadam 2008), as well as using self-stressing composites (Krstulovic-Opara and Thiedeman 2000, Shin and Andrawes 2010) are some of the methods for lateral post-tensioning. Another method for pre-stressing the composite columns is the active confinement of the fresh concrete, where by applying pressure to the fresh concrete, it is compressed and simultaneously, the steel tube is pre-tensioned in the circumferential direction (Nematzadeh *et al.* 2017a, b, c).Very little research has been conducted to investigate numerically the behavior of concrete columns with active confinement. One such study was performed by Moghaddam *et al.* (2010) with the use of the ABAQUS finite element program. They investigated the compressive behavior of the concrete confined with post-tensioned metal strips. In doing so, an analytical model was developed based on the experimental results of Moghaddam *et al.* (2010) to predict the compressive stress-strain curve of the confined concrete as a function of the confining level. This paper aims to perform a nonlinear analysis on the behavior of circular STCC columns having active confinement under axial compressive loading. To do so, a 3D finite element model is developed by means of the ABAQUS software (2012), which is then verified against the experimental results of Nematzadeh *et al.* (2017a, b) including 14 series of STCC specimens with different concrete compressive strengths, steel tube wall thicknesses, and pre-stressing levels. In this study, the parameters obtained from the previous research (Haghinejad and

Nematzadeh 2016) are utilized to define the behavior of concrete and steel materials, in which the compressed concrete mechanical properties (Nematzadeh and Naghipour 2012) are introduced. Also, the equivalent uniaxial stress-strain curve of the confined concrete is employed for the definition of the concrete behavior in the finite element model, in which the confinement effectiveness coefficient obtained from the experiments of Nematzadeh *et al.* (2017b) is applied. Moreover, to define the steel material behavior in the ABAQUS software, the steel multi-linear stress-strain curve is used. The parameters considered in this study for the verification purpose include the qualitative form of the stress-strain curve, and the compressive strengths corresponding to the initial peak point and the ultimate point. Finally, a parametric study is conducted to investigate the effect of various parameters including the concrete compressive strength, steel tube external diameter-to-wall thickness ratio, and pre-stressing level on the compressive behavior of STCC columns.

2. Summary of the experimental investigations

The experimental work performed by Nematzadeh *et al.* (2017a, b) includes studying the effect of the active confinement of fresh concrete by pre-stressing the steel tube on the compressive behavior of STCC stub columns; a summary of the experimental program of which is described here.

The actively-confined concrete specimens were prepared in 14 series with the variables of the concrete compressive strength, steel tube wall thickness, and pre-stressing level. Each series of the active specimens was divided into two groups, namely long-term pre-stressed steel tube-confined compressed concrete (LPSTC) and short-term pre-stressed steel tube-confined compressed concrete (SPSTC). In order to pre-stress the both active specimens, an axial pressure was applied to the fresh concrete using a pressure apparatus whose further details are given in Nematzadeh *et al.* (2017a, b, c). The difference between the two groups lies in the duration of this pressure application, which is 6 days and 15-30 min for the LPSTC and SPSTC specimens, respectively. In each test series, 12 steel tubes filled with fresh concrete and separated from each other by cylindrical covers were placed successively in the pressure apparatus. In this pre-stressing method, by applying pressure to the fresh concrete inside the steel tubes, the concrete becomes compressed and the steel tube becomes pretensioned laterally. The pre-stressing level was measured using horizontal strain gauges mounted at the mid-height of the steel tubes outer wall. The maximum hoop strain applied to the steel tube through compressing the fresh concrete was selected about 70% of the steel yielding strain; hence, the steel tube is in the elastic range after the end of pre-stressing and before the start of compressive loading. 28 days after the day of casting concrete, the confined specimens were subjected to axial compression by a compression testing machine. In order to determine the axial deformation of the specimens, two vertical LVDTs were employed, and to determine their lateral strain, two horizontal LVDTs were used in addition to the circumferential strain gauges. The LVDTs and strain gauges were mounted symmetrically on the both sides of

the specimens, and the mean of their recorded values was reported as the axial and lateral deformations. Note that in the STCC specimens, the axial load is applied only to the concrete core, and thus the vertical LVDTs are placed between the loading platens to measure the total axial deformation of the concrete core height taking into account the support conditions.

3. Actively-confined specimens modeling

3.1 Numerical simulation procedure

In this study, an innovative method was used for finite element modeling of STCC stub columns with active confinement. The proposed finite element model was verified with respect to the experimental results of the work of Nematzadeh *et al.* (2017a, b) involving 14 series of experimental STCC stub columns with various pre-stressing levels, concrete strengths, and steel tube external diameter-to-wall thickness ratio. After ensuring the accuracy of the modeling, a parametric study was performed to investigate the compressive behavior of these columns. It should be noted that the test specimens were prepared in the two groups of SPSTC and LPSTC specimens whose pre-stressing ratio was about 0.03, and ranging from 0.05 to 0.17, respectively.

3.2 Element type and mesh

In order to define the elements to model the specimens in the ABAQUS program, for a better performance and greater similarity with the actual behavior of the test specimens, the 3D solid element (C3D8R) was used, which decreases the computation time through reduced element integration. This element has eight nodes each having three translational degrees of freedom. One advantage of this element is the elimination of the shear lock problem caused by a finite element model with a very dense mesh in the program (Elsawaf 2012). In addition, considering the symmetry of the confined columns, the "structured" mesh was applied for the simulation. The meshing was performed such that all the meshes are distributed uniformly along the height and cross-section of the specimen.

3.3 Boundary conditions and load application

With respect to the geometrical symmetry of the test specimens as well as time-saving purposes, only 1/8 of the specimen was modeled in the ABAQUS finite element program. During the loading steps, the bottom surface of the composite section (symmetry surface along the height) was restrained only in the direction of displacement application. The top surface of the concrete core (loading surface) was restrained in all degrees of freedom except along the direction of displacement application, while the top surface of steel tube was free. Also, the lateral displacement of the symmetry surfaces of XZ and YZ was prevented in Y and X directions, respectively; hence, the center line of the modeled specimen was restrained in both X and Y directions. Fig. 1 shows a schematic view of the STCC column modeled in the software.
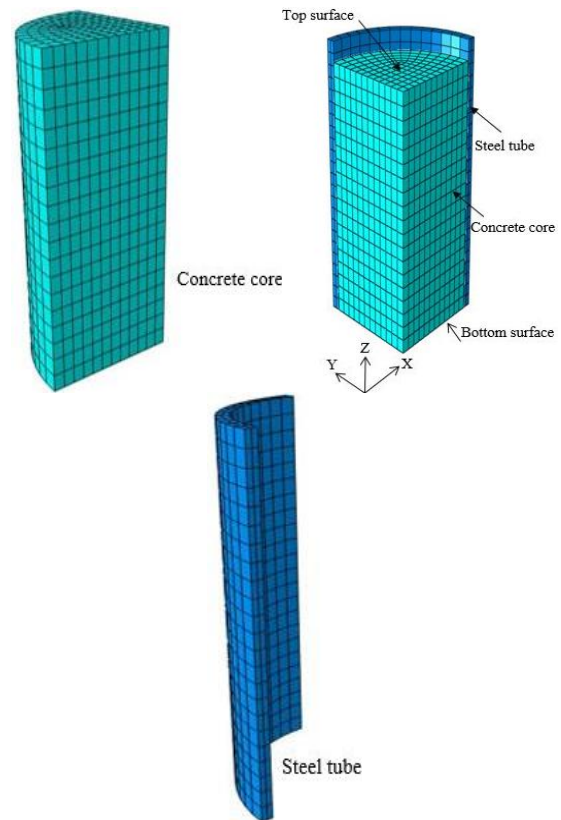

Fig. 1 Finite element mesh of STCC columns with active confinement

Loading the active specimens was conducted in three steps due to the presence of pre-stressing. In the first step, the steel tube, acting as a producer of active confining pressure around the concrete core, was subjected to a uniform radial pressure outward of the cylinder axis on the tube inner wall. In this step of the modelling of the pre-stressed specimens, the internal diameter of the steel tube is considered a little smaller than the concrete core diameter (without a change in the tube wall thickness), with the difference between the two depending on the pre-stressing level of the specimens and with the hoop strain of the steel tube at the beginning of axial loading being equal to the experimental one. To do so, the steel tube initial diameter was selected based on the relationships given in the classical strength of materials. Applying the pressure to the inner wall of the steel tube results in its internal diameter to become larger than the concrete core diameter thus the two become separated; however, the pressure value is such that the steel tube stays in the elastic range. It should be noted that in this step, there is no interaction between the concrete and steel. In the second loading step, with the linear reduction of the applied radial pressure to zero and using the steel elastic properties, the steel tube tends to return to the initial condition. Once the inner surface of the steel tube comes into contact with the lateral surface of the concrete core, because of the interaction defined between the two surfaces in this step, the steel tube and the concrete core experience surface to surface contact. As a result, a hoop tensile stress is developed in the steel tube, leading to the application of an initial lateral pressure to the concrete core
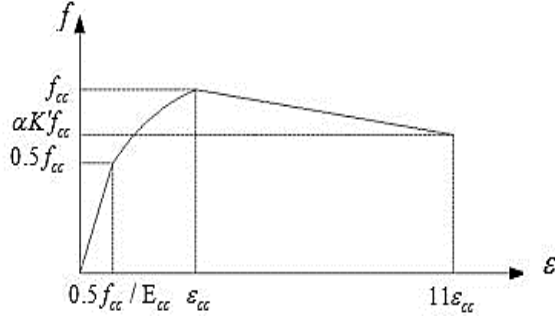
Fig. 2 Uniaxial stress-strain curve of actively-confined concrete

and thus pre-stressing the confined specimens at the beginning of the third step. The lateral loading and unloading in the first and second loading steps are conducted by defining an appropriate amplitude, which is in fact a history of the given loading. This means that the lateral load starts from zero and reaches its ultimate value at the end of the analysis time, and again reaches zero after its ultimate value. At the final step, using General Static Method, the uniform static external loading is applied through applying a direct displacement on the nodes located on the top surface of the concrete core, and subsequently, the specimen undergoes axial compression.

3.4 Modeling of the confined concrete

3.4.1 Stress-strain curve

Since the test specimens used in this study were under an initial confining pressure prior to experiencing the compressive axial load, the confined concrete core of these specimens behaved in a different way than that of the passively confined specimens. The uniaxial stress-strain curve of the actively-confined concrete is plotted in Fig. 2, in which the first region is considered as linear continuing to half the compressive strength of the confined concrete ($0.5 f_{cc}$). The compressive strength of the confined concrete (f_{cc}) and its corresponding strain (ε_{cc}) for active STCC specimens can be obtained from Eqs. (1) and (2) based on the experimental results of Nematzadeh *et al.* (2017b) and Mander *et al.* (1988), respectively.

$$f_{cc} = \left(2.31 \left(\frac{f_l}{f_{cp}} \right)^{0.7} \left(1 + \gamma P_r \right) f_{cp} \right) + f_{cp} \tag{1}$$

$$\varepsilon_{cc} = \left(5 \left(\frac{f_{cc}}{f_{cp}} - 1 \right) + 1 \right) \varepsilon_c \tag{2}$$

where ε_c is the unconfined concrete strain corresponding to the maximum stress and is considered as 0.003, and γ is a constant value equal to 1.0 and 2.9 for LPSTC and SPSTC specimens, respectively. In addition, f_{cp} denotes the compressed concrete compressive strength, the value of which is calculated based on the uncompressed concrete strength (f_c) using Eqs. (3) and (4) for LPSTC and SPSTC specimens, respectively (Nematzadeh and Naghipour 2012).

$$f_{cp} = -0.0331 f_c^2 + 3.185 f_c \tag{3}$$

$$f_{cp} = -0.0370 f_c^2 + 3.217 f_c \tag{4}$$

Furthermore, the curve slope in the linear region is denoted by E_{cc} (the initial modulus of elasticity of the confined concrete) and determined by utilizing the experimental equations proposed in Nematzadeh and Naghipour (2012) as follows

$$E_{cc} = 3496.5 \sqrt{f_{cp}} + 15932 \tag{5}$$

where E_{cc} and f_{cp} are expressed in MPa.

In Eq. (1), f_l is the lateral confining pressure applied to the concrete core, the value of which can be determined using the empirical relationship, i.e., Eq. (6), obtained by matching the results of modeling and those of the experiments. This equation suggests that the value of f_l is independent of the concrete compressive strength; instead, it is a function of the tube external diameter-to-wall thickness ratio (D/t) and steel yield stress (f_y).

$$\frac{f_l}{f_y} = 0.034366 - 0.000452 \left(\frac{D}{t} \right) \tag{6}$$

Furthermore, P_r is the pre-stressing ratio which is calculated using

$$P_r = \frac{P_f}{f_{cp}} \tag{7}$$

where P_f is the pre-stressing level, i.e., the lateral pressure applied to the concrete core prior to the compression test, which is obtained in terms of the initial hoop strain of the steel tube using the classical strength of materials' equation, $P_f = 2 E_s \varepsilon_i t / (D - 2t)$, where E_s and ε_i are the modulus of elasticity and initial strain (pre-stressing level) of the steel tube, respectively.

The second region in the actively-confined specimen's stress-strain curve starting from the end of the linear region and continuing up to f_{cc} is obtained from Eq. (8) proposed by Saenz (1964) written as

$$f = \frac{E_{cc} \varepsilon}{1 + (R + R_E - 2)(\frac{\varepsilon}{\varepsilon_{cc}}) - (2R - 1)(\frac{\varepsilon}{\varepsilon_{cc}})^2 + R(\frac{\varepsilon}{\varepsilon_{cc}})^3} \tag{8}$$

where f and ε are uniaxial stress and strain of the confined concrete, respectively, and R_E and R are modular ratio and ratio relation, respectively, which are calculated as follows

$$R_E = \frac{E_{cc} \varepsilon_{cc}}{f_{cc}} \tag{9}$$

$$R = \frac{R_E (R_\sigma - 1)}{(R_\varepsilon - 1)^2} - \frac{1}{R_\varepsilon} \tag{10}$$

where R_σ and R_ε are stress ratio and strain ratio, respectively, which define the curve shape after the peak

point (descending branch) and, as recommended by Hu and Schnobrich, are both taken equal to 4.0 (Hu and Schnobrich 1989).

The third region of the actively-confined concrete stress-strain curve is also considered linear with the end strain and stress being $11\varepsilon_{cc}$ and $aK'f_{cc}$, respectively. The K' parameter is given as Eqs. (11) and (12) based on the empirical equations proposed for the passively-confined specimens (Haghinejad and Nematzadeh 2016). A correction factor, a, is introduced in the equations in order to obtain a better match between the finite element and experimental results in the specimens experiencing active confinement. In this study, the value of 0.9 is obtained for the factor.

$$K' = \left(0.0264865 - 0.0003861\frac{D}{t} \right)(85 - 0.625f_c) \tag{11}$$

$$24.2 \le \frac{D}{t} \le 29.75, 16.7 \le f_c \le 52.6$$

$$K' = \left(0.0169283 - 0.0000662\frac{D}{t} \right)(85 - 0.625f_c) \tag{12}$$

$$29.75 \le \frac{D}{t} \le 57.5, 16.7 \le f_c \le 52.6$$

3.4.2 Yield surface

Concrete yield surface can be investigated by well-known yield functions including Tresca, von Mises, Mohr-Coulomb, Drucker-Prager, and Willam-Warnke (Chen 1982). In this study, in order to model the confined concrete yield surface, the linear Drucker-Prager criterion, which has a direct relationship with hydrostatic pressure, was employed. The linear Drucker-Prager yield surface available in the ABAQUS library is given as

$$F = q - p\tan\beta - d \tag{13}$$

where p and q are the equivalent compressive stress and Mises equivalent stress, respectively. In addition, parameter d specifies the cohesion, and β the friction angle of the material; the value of the latter is considered $20°$ based on the results of the previous work (Haghinejad and Nematzadeh 2016).

To determine the inelastic deformations, a linear flow potential function, G, is used which is written as

$$G = t - p\tan\psi \tag{14}$$

where t is the shear strength, and Ψ is the volumetric dilation angle which is measured in high confining pressures and considered equal to $35°$ in this study. To be able to apply the Drucker-Prager yield criterion in the ABAQUS, it is necessary to assign the values of the other effective parameters; one of which being the factor K defined as the ratio of shear strength in biaxial compression to that in triaxial one. To ensure that the yield surface in the deviatoric plane (the plane perpendicular to the bisector of the stress axes) remains convex, it is necessary that $0.778 \le K \le 1$. Regarding the above limitation, it can be said that the yield surface shape in the deviatoric plane is circular with the same value of yield stress within it (conventional Drucker-Prager model). Otherwise, the shape

Table 1 Properties of the active STCC specimens (Nematzadeh *et al.* 2017a, b)

Specimen identifier	t (mm)	D/t	L_c (mm)	f_c (MPa)	Initial hoop strain of steel tube in $\mu\varepsilon$ (Confining pressure in MPa)
L25P350-2.5	2.5	24.2	125.5	28.2	233.3(4.4)
S25P350-2.5	2.5	24.2	125.7	28.2	98.4(1.9)
L25P950-1.5	1.5	39.0	124.5	31.7	729.4(8.3)
S25P950-1.5	1.5	39.0	124.7	31.7	179.0(2.0)
L25P650-1.5	1.5	39.0	125.3	28.3	399.7(4.5)
S25P650-1.5	1.5	39.0	125.5	28.3	100.7(1.1)
L35P650-1.5	1.5	39.0	126.6	42.4	400.5(4.5)
S35P650-1.5	1.5	39.0	127.2	42.4	119.5(1.4)
L15P650-1.5	1.5	39.0	127.3	20.5	400.5(4.5)
S15P650-1.5	1.5	39.0	127.9	20.5	119.5(1.4)
L25P950-2.5	2.5	24.2	123.2	30.0	596.0(11.3)
S25P950-2.5	2.5	24.2	124.5	30.0	168.7(3.2)
L50P650-2.5	2.5	24.2	125.0	50.5	321.8(6.1)
S50P650-2.5	2.5	24.2	126.4	50.5	115.3(2.2)
L15P550-2.5	2.5	24.2	127.6	16.7	267.8(5.1)
S15P550-2.5	2.5	24.2	127.3	16.7	109.3(2.1)
L35P550-2.5	2.5	24.2	126.3	37.1	267.8(5.1)
S35P550-2.5	2.5	24.2	127.4	37.1	109.3(2.1)
L25P500-2.5	2.5	24.2	125.2	27.2	268.9(5.1)
S25P500-2.5	2.5	24.2	127.0	27.2	64.5(1.2)
L25P650-2.0	2.0	29.8	126.1	27.2	336.2(5.1)
S25P650-2.0	2.0	29.8	125.6	27.2	80.6(1.2)
L45P650-1.5	1.5	39.0	127.2	45.4	343.0(3.9)
S45P650-1.5	1.5	39.0	126.5	45.4	203.3(2.3)
L25P2000-1.0	1.0	57.5	124.3	25.9	1159.0(8.8)
S25P2000-1.0	1.0	57.5	126.4	25.9	420.3(3.2)
L47P650-1.5	1.5	39.0	125.2	46.9	315.2(3.6)
S47P650-1.5	1.5	39.0	127.4	46.9	90.5(1.0)

of the yield surface is not circular anymore with various values of the yield stress (extended Drucker-Prager model). In this study, for the purpose of modeling in the ABAQUS, K was considered as 0.8.

3.5 Modeling of steel tube

To define the steel material, the experimental trilinear stress-strain model was employed. Using the "Elastic" option available in the ABAQUS program library allows the definition of the steel material elastic behavior in the program, in which the values of 210 GPa and 0.28 were assigned to the Young's modulus and Poisson's ratio, respectively. In addition, the steel inelastic behavior involving the yield and strain hardening stages can be expressed by employing the "Plastic" option in the program library. The required parameters to define the steel inelastic behavior include the yield stress (f_y), ultimate stress (f_{su}), elastic strain (ε_e), strain at the beginning of strain hardening (ε_p), and ultimate strain (ε_{su}), the values of which are 339 MPa, 480 MPa, 0.0016, 0.0139 and 0.114, respectively, in accordance with the experimental results of Nematzadeh *et al.* (2017a, b).

3.6 Concrete-steel tube interface modeling

In order to simulate the interactions between the components in contact, the Contact function of the ABAQUS capable of mechanically simulating two deformable objects at the interface is employed. To reduce the computation time, all the available contact relationships were defined as "surface-to-surface" contact with slip possibility, in which the inner wall of the steel tube and the outer surface of the concrete core are considered as "master" and "slave" surfaces, respectively. In this

Table 2 Finite element analysis results of LPSTC and SPSTC specimens as well as experimental results (Nematzadeh *et al.* 2017a, b)

Specimen identifier	Initial peak point strength (MPa)		EXP/FEA	Failure point strength (MPa)		EXP/FEA
	EXP	FEA		EXP	FEA	
L25P350-2.5	166.8	159.2	1.05	230.3	225.3	1.02
S25P350-2.5	163.5	157.1	1.04	224.8	220.5	1.02
L25P950-1.5	134.9	134.4	1.00	130.0	142.5	0.92
S25P950-1.5	131.1	130.2	1.01	130.5	142.6	0.91
L25P650-1.5	127.0	128.3	0.99	133.0	146.1	0.91
S25P650-1.5	122.6	125.2	0.98	129.2	144.8	0.89
L35P650-1.5	140.3	141.6	0.99	132.6	137.5	0.96
S35P650-1.5	139.9	135.0	1.04	138.5	144.1	0.96
L15P650-1.5	104.5	114.9	0.91	127.4	146.0	0.87
S15P650-1.5	102.7	113.3	0.91	125.4	144.7	0.87
L25P950-2.5	171.6	166.0	1.03	232.6	225.3	1.03
S25P950-2.5	170.6	161.5	1.06	239.2	224.9	1.06
L50P650-2.5	200.4	175.0	1.14	234.2	211.7	1.11
S50P650-2.5	188.4	165.6	1.14	240.1	220.3	1.09
L15P550-2.5	141.8	137.1	1.03	212.4	215.8	0.98
S15P550-2.5	139.1	136.5	1.02	221.6	222.4	1.00
L35P550-2.5	178.9	170.3	1.05	216.8	218.1	0.99
S35P550-2.5	172.3	165.6	1.04	226.2	222.5	1.02
L25P500-2.5	158.7	158.6	1.00	231.5	224.4	1.03
S25P500-2.5	151.2	156.3	0.97	231.2	223.4	1.04
L25P650-2.0	142.6	143.8	0.99	175.3	176.6	0.99
S25P650-2.0	141.9	140.3	1.01	182.3	182.8	1.00
L45P650-1.5	147.8	141.9	1.04	139.2	140.0	0.99
S45P650-1.5	142.6	136.1	1.05	134.0	143.7	0.93
L25P2000-1.0	117.0	102.5	1.14	93.6	98.1	0.95
S25P2000-1.0	108.8	100.9	1.08	94.1	97.7	0.96
L47P650-1.5	150.6	142.4	1.06	135.7	130.2	1.04
S47P650-1.5	141.0	134.2	1.05	130.5	136.1	0.96

(a) Peak strength   (b) Failure strength

Fig. 3 Compressive strength results of finite element versus experimental for LPSTC specimens at the points of initial peak and failure

(a) Peak strength   (b) Failure strength

Fig. 4 Compressive strength results of finite element versus experimental for SPSTC specimens at the points of initial peak and failure

simulation, normal and tangential contact interactive properties are utilized. The "Hard contact" option is defined for the interface in normal contact, which allows for the separation of the interface during tension and its impermeability during compression. Tangential contact is simulated using Coulumb friction model, and the penalty method is used to formulate the tangential friction behaviour. For short STCC stub columns, a slip exists between the concrete core and steel tube due to applying load only to the concrete core. Therefore, the compressive behaviour of the column is sensitive to the choice of proper friction coefficient between concrete and steel. In this research, the friction coefficient of 0.65 was considered in the tangential direction between the contact surfaces of the concrete core and steel tube through matching the finite element results with those obtained from the experiments.
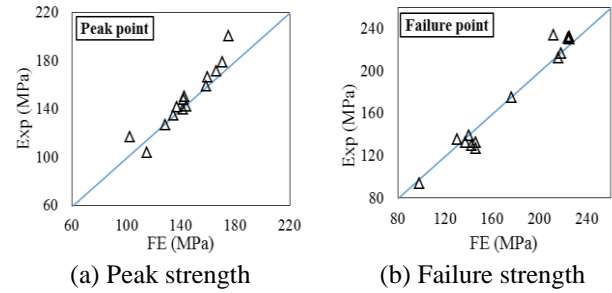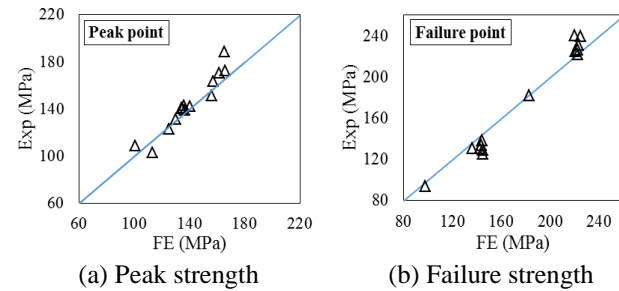
4. Verification of the finite element model

To verify the proposed finite element model, the active STCC specimens tested in the work of Nematzadeh *et al.* (2017a, b) were simulated in the ABAQUS program, and then, the results were compared with those of the experiments, which include the compressive strength at the initial peak point (the point corresponding to the relative maximum stress) and the failure point, as well as axial and lateral stress-strain curves. A total of 14 series of active STCC specimens were compared with the proposed finite element model; the characteristics and identifications of which are presented in Table 1. Each of these series comprised of six test specimens divided into the two groups of LPSTC and SPSTC specimens.

The results obtained from the finite element modeling and experiments are given in Table 2 where the ratio of the experimental to finite element analysis results for the compressive strength at the initial peak point and failure point is, on average, 1.03 and 0.98, respectively, suggesting an appropriate prediction of the compressive strength by the finite element model.

For a better comparison, the compressive strengths obtained from the finite element model versus those of the experiments for the LPSTC and SPSTC specimens are shown in Figs. 3 and 4, respectively. As can be seen, the obtained points are distributed properly near the bisector line, indicating a small difference between the finite element and experimental results for the active specimens.

The axial and lateral stress-strain curves for the proposed finite element model along with the experimental results are plotted in Fig. 5. Regarding the figure, it can be found that the proposed finite element model has a high accuracy and reliability for the behavior prediction of the active STCC specimens.
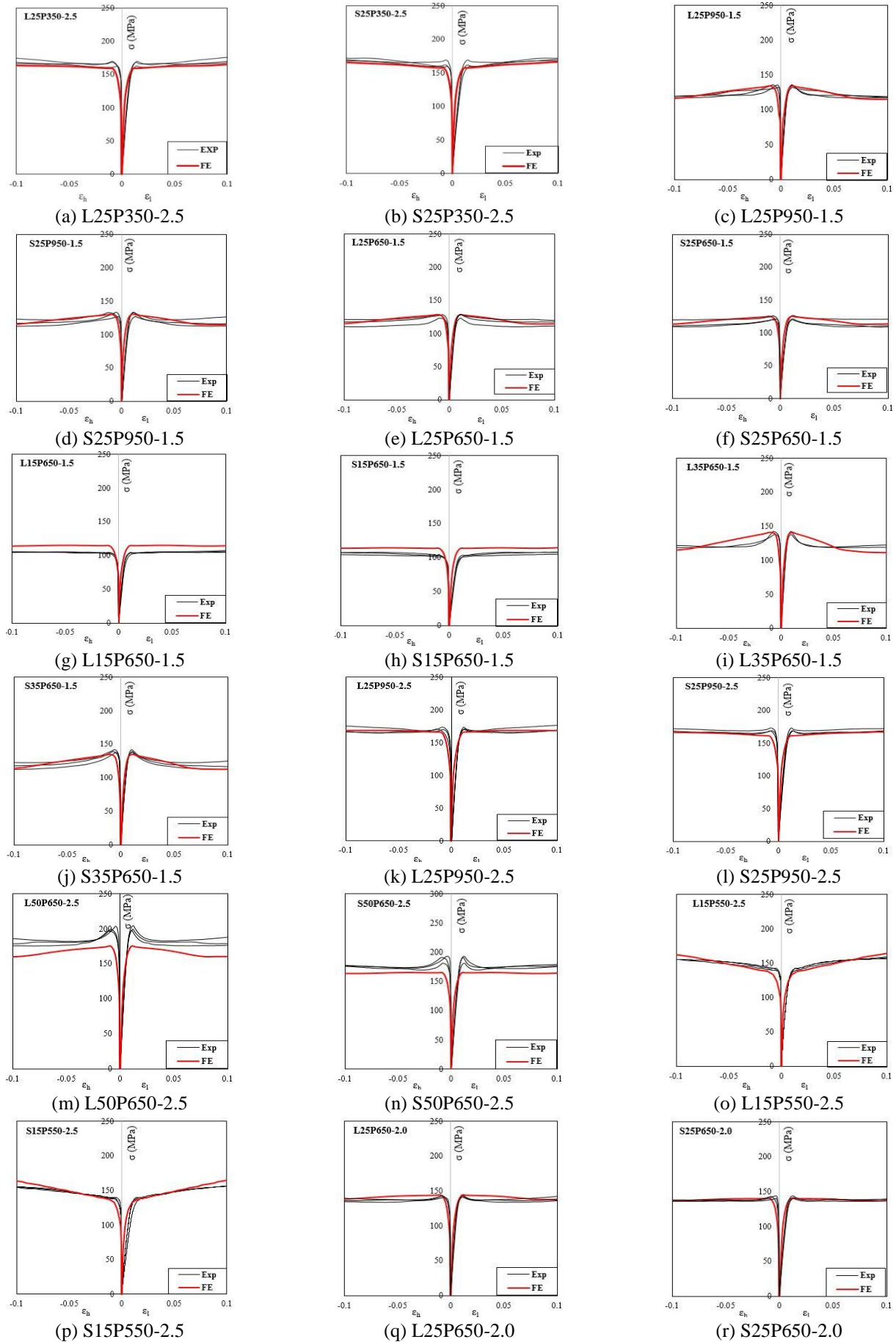
(a) L25P350-2.5   (b) S25P350-2.5   (c) L25P950-1.5

(d) S25P950-1.5   (e) L25P650-1.5   (f) S25P650-1.5

(g) L15P650-1.5   (h) S15P650-1.5   (i) L35P650-1.5

(j) S35P650-1.5   (k) L25P950-2.5   (l) S25P950-2.5

(m) L50P650-2.5   (n) S50P650-2.5   (o) L15P550-2.5

(p) S15P550-2.5   (q) L25P650-2.0   (r) S25P650-2.0

Fig. 5 Axial and lateral stress-strain curve of the confined specimens

(a) Yielding strength of $S_{fc-1-Pr}$ (b) Peak strength of $S_{fc-1-Pr}$ (c) Failure strength of $S_{fc-1-Pr}$

(d) Yielding strength of $S_{fc-3-Pr}$ (e) Peak strength of $S_{fc-3-Pr}$ (f) Failure strength of $S_{fc-3-Pr}$
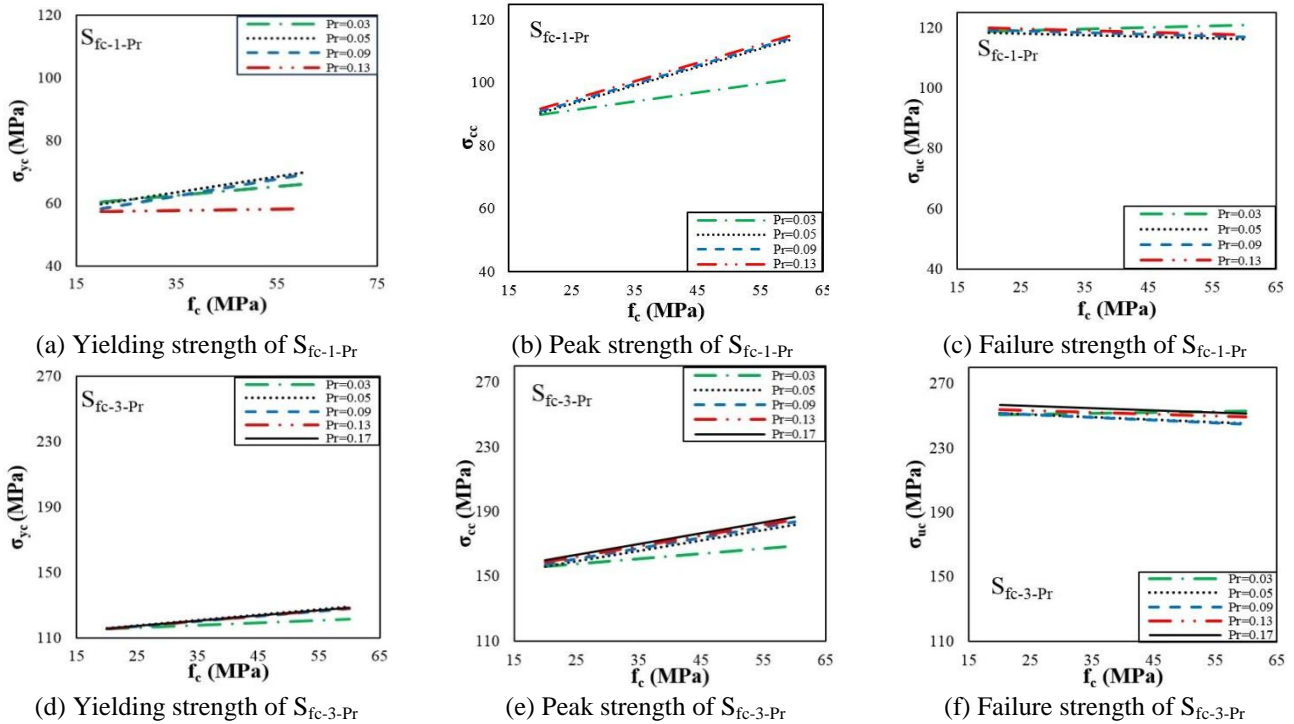
Fig. 6 Compressive strength of the active STCC specimens versus the concrete compressive strength

Table 3 The properties of the specimens in the parametric study

f_c (MPa)	t (mm)	D/t	P_r	D_c (mm)	L_c (mm)	L_s (mm)
20, 60	1.0 , 3.0	57.5, 20.5	0.03, 0.05, 0.09, 0.13, 0.17	55.5	63	68

Table 4 Results of the parametric study

Specimen identifier	σ_{yc} (MPa)	σ_{cc} (MPa)	σ_{uc} (MPa)	Specimen identifier	σ_{yc} (MPa)	σ_{cc} (MPa)	σ_{uc} (MPa)
$S_{20-3-0.3}$	115.25	156.12	250.93	$S_{60-1-0.3}$	66.22	101.18	120.93
$S_{20-3-0.5}$	115.73	155.99	251.69	$S_{60-1-0.5}$	69.83	113.67	116.36
$S_{20-3-0.9}$	115.58	157.42	251.51	$S_{60-1-0.9}$	69.15	114.38	116.96
$S_{20-3-0.13}$	115.57	158.76	254.12	$S_{60-1-0.13}$	58.27	115.04	117.37
$S_{20-3-0.17}$	115.56	160.03	256.68	$S_{60-3-0.3}$	121.55	168.88	252.83
$S_{20-1-0.3}$	60.38	89.89	118.85	$S_{60-3-0.5}$	128.99	181.92	245.16
$S_{20-1-0.5}$	59.72	90.32	118.43	$S_{60-3-0.9}$	127.73	183.52	244.74
$S_{20-1-0.9}$	58.23	90.96	119.26	$S_{60-3-0.13}$	128.00	185.11	249.46
$S_{20-1-0.13}$	57.52	91.58	120.05	$S_{60-3-0.17}$	128.23	186.69	251.61
$S_{20-1-0.17}$	45.89	92.21	120.85				

(a) f_c=20 MPa

(b) f_c=60 MPa

Fig. 7 Axial stress-strain curve of the active STCC specimens

5. Parametric study

After verifying the proposed finite element model as well as ensuring its suitability for modeling active STCC specimens, a parametric study was performed to investigate the effect of various parameters including the uncompressed concrete compressive strength (f_c), steel tube external diameter-to-wall thickness ratio (D/t), and pre-stressing ratio (P_r) on the compressive behavior of the pre-stressed STCC columns. A total of 19 active STCC specimens were
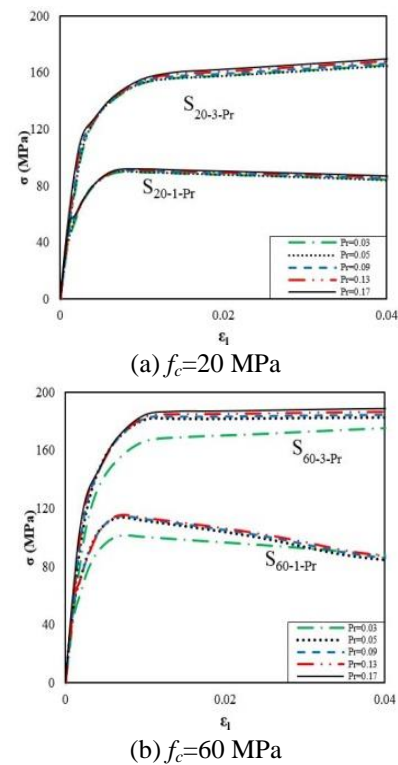
selected for the parametric study; their geometrical and mechanical properties are presented in Table 3, in which D_c and L_c are the diameter and length of the concrete core, respectively, and t and L_s are the wall thickness and length of steel tube, respectively. In all the studied specimens, a trilinear stress-strain curve of steel with the previous
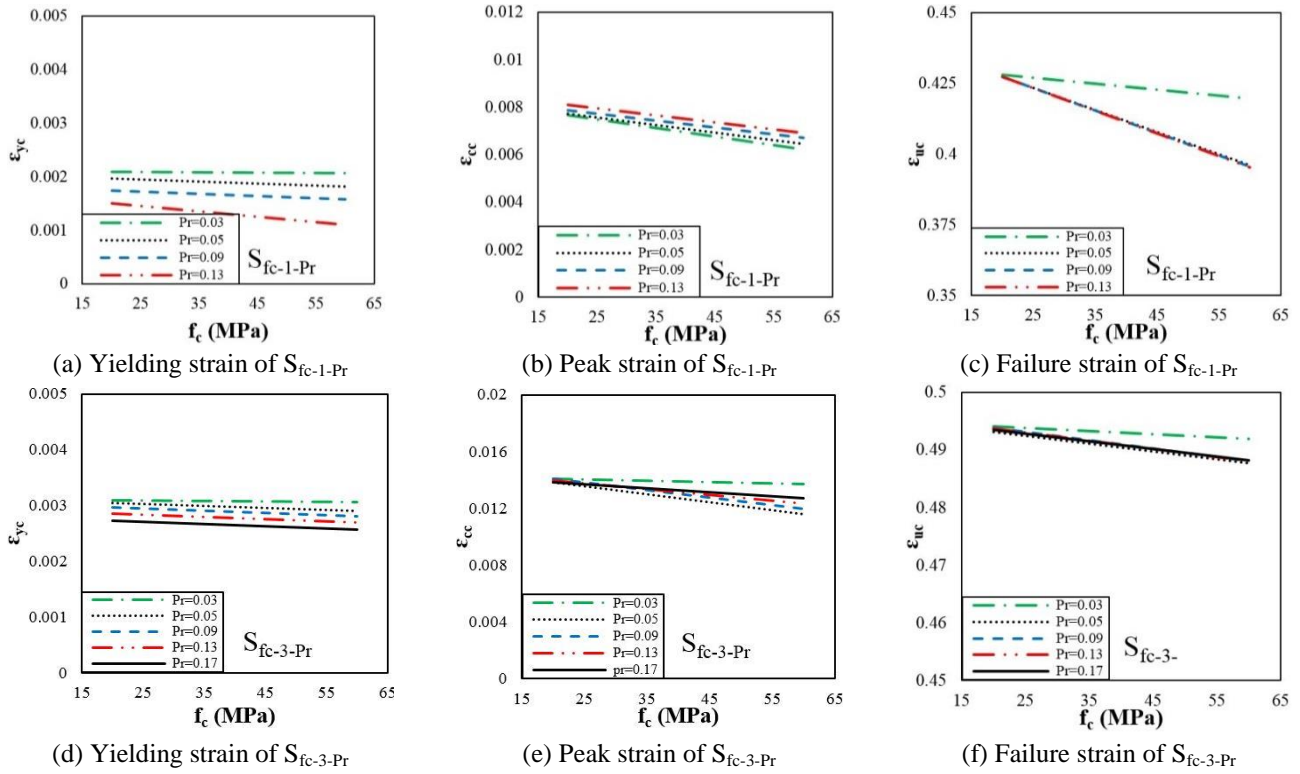
(a) Yielding strain of $S_{fc-1-Pr}$ (b) Peak strain of $S_{fc-1-Pr}$ (c) Failure strain of $S_{fc-1-Pr}$

(d) Yielding strain of $S_{fc-3-Pr}$ (e) Peak strain of $S_{fc-3-Pr}$ (f) Failure strain of $S_{fc-3-Pr}$

Fig. 8 Axial strain of the active STCC specimens versus the concrete compressive strength

(a) Yielding point, f_c=20 MPa   (b) Peak point, f_c=20 MPa   (c) Failure point, f_c=20 MPa

(d) Yielding point, f_c=60 MPa   (e) Peak point, f_c=60 MPa   (f) Failure point, f_c=60 MPa
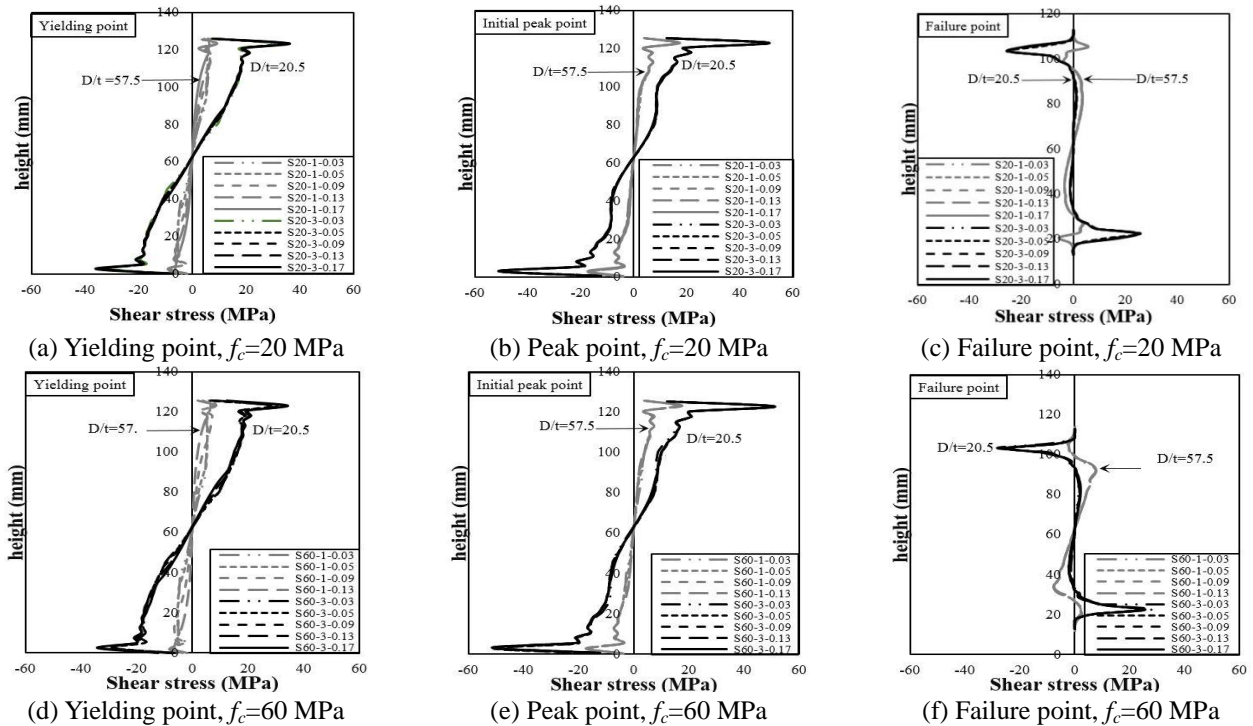
Fig. 9 Shear stress at the concrete-steel interface of the active STCC specimens

mechanical properties was used.

For the purpose of identifying the specimens, name assignment for each one was carried out as $S_{fc-t-Pr}$, in which after the letter S, the values for the uncompressed concrete compressive strength, tube wall thickness, and pre-stressing ratio are replaced. For example, the specimen $S_{20-3-0.17}$ represents a specimen possessing the concrete compressive

strength of 20 MPa, steel tube wall thickness of 3 mm, and pre-stressing ratio of 0.17. Furthermore, for identifying a group of the specimens with the same value for one of the parameters of interest, the letter or letters representing that parameter is replaced in the nomination. After modeling the active STCC specimens, the analysis results including the compressive strength, axial stress-strain curve of the

(a) Yielding point, f_c=20 MPa   (b) Peak point, f_c=20 MPa   (c) Failure point, f_c=20 MPa

(d) Yielding point, f_c=60 MPa   (e) Peak point, f_c=60 MPa   (f) Failure point, f_c=60 MPa
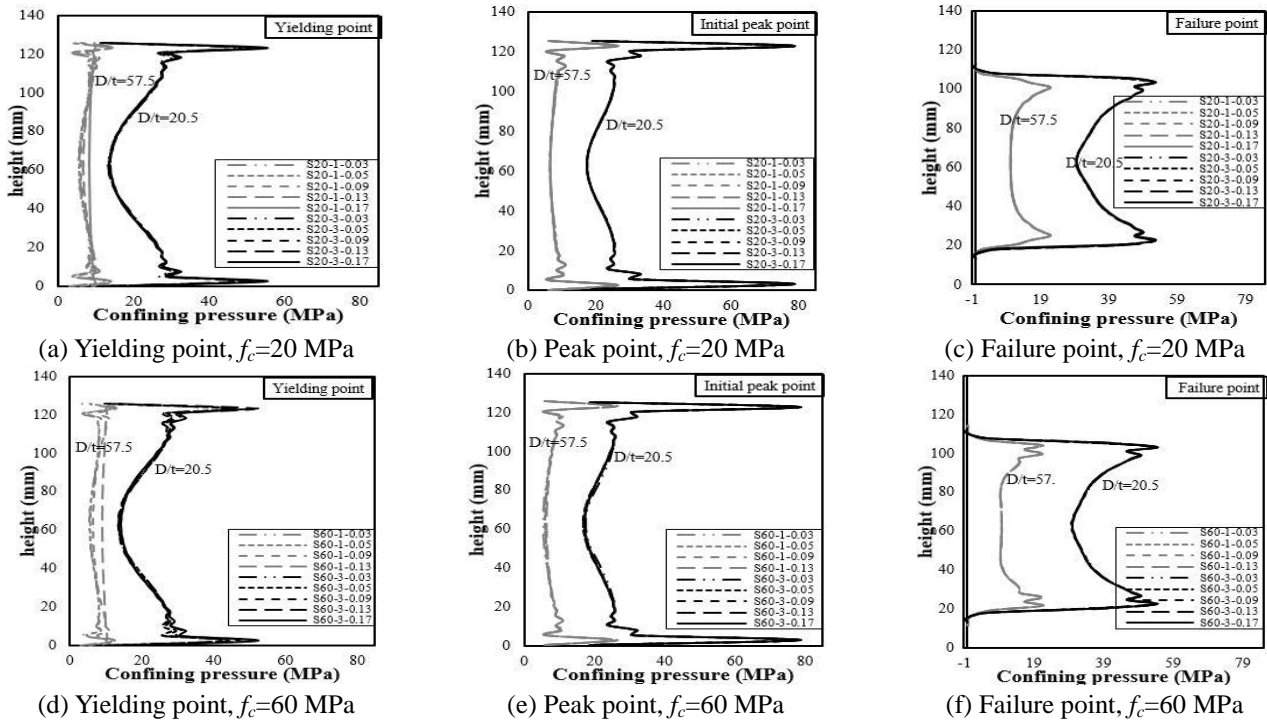
Fig. 10 Confining pressure at the concrete-steel interface of the active STCC specimens

composite section, and interaction between the concrete and steel were investigated. The results obtained for the compressive strength at the steel yielding point (σ_{yc}), initial peak point (σ_{cc}), and failure point (σ_{uc}) for the active specimens are given in Table 4.

5.1 Compressive strength of the composite section

The effect of the concrete compressive strength on the compressive strength of the composite column for different pre-stressing ratios at the points of steel yielding (σ_{yc}), initial peak (σ_{cc}), and failure (σ_{uc}) is demonstrated in Fig. 6.

With respect to Fig. 6, it is observed that in all the specimens, with an increase in the concrete compressive strength at the steel yield and initial peak points, the composite column compressive strength increases, while at the failure point, it either remains constant or decreases, which is due to the quicker failure of the specimens with higher concrete compressive strengths. Additionally, with decreasing the steel tube diameter-to-wall thickness ratio, the compressive strength of the composite section increases due to the increasing confining pressure. It can also be seen in Fig. 6 that increasing the pre-stressing ratio at high levels has no significant effect on the compressive strength of the composite column.

5.2 Axial stress-strain curve of the composite section

The axial stress-strain curve of the active STCC specimens is demonstrated in Fig. 7, in which the effect of the parameters of pre-stressing ratio, concrete strength, and steel tube outer diameter-to-wall thickness ratio on the compressive behavior of the composite sections can be observed.

Considering that a major portion of the compressive

load-carrying capacity in STCC specimens belongs to the concrete core, it can be seen in Fig. 7 that with increasing the concrete strength, the load-carrying capacity of the composite sections also increases. In addition, it can be seen that as the steel tube outer diameter-to-wall thickness ratio decreases, the strength of the STCC composite specimens increases as a result of the increasing confining pressure. Also, it is observed, in general, that variations in the pre-stressing ratio have a negligible effect on the compressive stress-strain behavior of the active specimens, such that the LPSTC and SPSTC specimens having active confinement behave in almost the same way, except for the composite specimens with a high concrete strength in which the stress-strain curve of the long-term pre-stressed active specimens is located higher than that of the short-term ones. The reason for this is the fact that the difference between the compressive strength values of the LPSTC and SPSTC specimens at high levels of f_c is greater than that at low levels.

5.3 Axial strain of the composite section

Fig. 8 shows the axial strain values of the actively-confined specimens at the points of steel yielding (ε_{yc}), initial peak (ε_{cc}), and failure (ε_{uc}) for different values of the concrete strength, steel tube outer diameter-to-wall thickness ratio, and pre-stressing ratio.

From the figure, it is observed that the axial strain in the SPSTC specimens is higher than that of the LPSTC ones, with this difference being more evident at the failure point. In addition, it is seen that the axial strain of the composite sections decreases with increasing the concrete strength; the reason to which can be attributed to an increase in the stiffness and a more brittle compressive behavior of the

composite column. Furthermore, at the steel yielding point, the axial strain decreases as the pre-stressing ratio increases since the steel tube yielding occurs earlier, and at the failure point, due to the reduced strain capacity, the steel tube failure occurs at lower strains.

5.4 Interface shear stress

The shear stress at the concrete core-steel tube interface in the longitudinal direction at the points of steel yielding, initial peak, and failure for the actively-confined specimens is demonstrated in Fig. 9. Regarding this figure, it can be found that the shear stress distribution in the longitudinal direction is non-uniform with the maximum value appearing at the two ends of the column, and by moving toward the mid-height of the specimens, it decreases and tends to zero. In addition, it can be seen that as the steel tube external diameter-to-wall thickness ratio decreases, the interface shear stress increases. However, the interface longitudinal shear stress is not affected by the increase in the concrete compressive strength and pre-stressing ratio.

5.5 Confining pressure

Distribution of the confining pressure applied to the concrete core by the steel tube in the longitudinal direction of the composite sections at the points of steel yielding, initial peak, and failure is shown in Fig. 10, where it can be seen that the maximum confining pressure occurs at the two ends of the composite columns. Moreover, it is observed that increasing the steel tube wall thickness leads to an increase in the confining pressure applied to the concrete, while increasing the concrete compressive strength as well as the pre-stressing ratio has no effect on it. However, an increase in the pre-stressing ratio at the yield point have a small effect on increasing the confining pressure due to the faster yielding of the steel tube.

6. Proposed equations for compressive strength of actively-confined concrete

By using the nonlinear regression analysis of the FE model results obtained from this study, Eqs. (15) and (16) are proposed for the compressive strength at the initial peak and ultimate point, respectively, of the STCC stub columns with active confinement.

$$f_{cc} / f_{cp} = 1 + (5.7 + 0.5\alpha P_r)(\frac{t\,f_y}{D\,f_{cp}})^{0.87} \qquad (15)$$

$$f_{cc} / f_{cp} = 1 + (12.4 + 0.4\alpha P_r)(\frac{t\,f_y}{D\,f_{cp}})^{1.4} \qquad (16)$$

where α is 1.0 and 2.9 for LPSTC and SPSTC specimens, respectively, and f_{cc}/f_{cp} is the ratio of compressive strength of actively-confined concrete to that of the unconfined compressed concrete. It should be noted that the above equations are applicable for actively-confined concrete

columns with a minimum pre-stressing level, and cannot be used for $P_r=0$ (as a passive confinement).

7. Conclusions

In this study, an appropriate nonlinear finite element model with the purpose of analyzing the STCC stub columns with active confinement was presented, in which a new stress-strain relationship for the actively-confined concrete was proposed. It was revealed that the results of the finite element and experiments were in a good agreement. After verifying the proposed model, a parametric study was conducted to investigate the effect of the parameters including concrete compressive strength, steel tube wall thickness, and pre-stressing level on the compressive behavior of the STCC columns. Based on the analytical results, the following conclusions can be drawn.

• The axial strain of the SPSTC specimens is higher than that of the LPSTC specimens at the points of yielding, initial peak, and failure, with this difference being more evident at the failure point. Moreover, increasing the pre-stressing ratio results in a reduction in the yielding and failure strain capacity of the steel tube.

• As the value of f_c increases, the compressive strength of the composite column at the points of yielding and initial peak in all the active specimens tends to increase, while being almost constant or decreasing at the failure point. Furthermore, with decreasing the D/t ratio, which leads to an increase in the confining pressure, the compressive strength of the composite section increases.

• Increasing the pre-stressing level has a significant effect on the compressive strength of the active STCC specimens having high-strength concrete, while in other specimens, it has a negligible effect on the composite compressive strength.

• The interface shear stress and lateral confining pressure along the height of the active STCC specimens are distributed non-uniformly, with the maximum and minimum values occurring at the two ends and at the mid-height of the specimens, respectively. Furthermore, the both parameters of interest are not affected by f_c, while increasing the D/t significantly affects them. In addition, the pre-stressing ratio has no effect on the interface shear stress and confining pressure of the active STCC specimens.

References

ABAQUS 6.12 Documentation (2012), *ABAQUS Users and Analysis Users Manual*, Rhode Island, U.S.A.

Chang, X., Huang, C.K. and Chen, Y.J. (2009), "Mechanical performance of eccentrically loaded prestressing concrete filled circular steel tube columns by means of expansive cement", *Eng. Struct.*, **31**(11), 2588-2597.

Chen, W.F. (1982), *Plasticity in Reinforced Concrete*.

Ellobody, E., Young, B. and Lam, D. (2006), "Behaviour of normal and high strength concrete-filled compact steel tube circular stub columns", *J. Constr. Steel Res.*, **62**(7), 706-715.

Elsawaf, S. (2012), "Robustness of connections to concrete-filled steel tubular columns under fire during heating and cooling",

Ph.D. Dissertation, University of Manchester, Manchester, U.K.

Feeser, L.J. and Chinn, J. (1962), "Strength and stiffness of spirally prestressed concrete cylinders", *PCI J.*, **7**(3), 55-62.

Gupta, P.K., Verma, V.K., Khaudhair, Z.A. and Singh, H. (2015), "Effect of tube area on the behavior of concrete filled tubular columns", *Comput. Concrete*, **15**(2), 141-166.

Haghinejad, A. and Nematzadeh, M. (2016), "Three-dimensional finite element analysis of compressive behavior of circular steel tube-confined concrete stub columns by new confinement relationships", *Lat. Am. J. Sol. Struct.*, **13**(5), 916-944.

Han, L.H., Yao, G.H., Chen, Z.B. and Yu, Q. (2005), "Experimental behaviour of steel tube confined concrete (STCC) columns", *Steel Compos. Struct.*, **5**(6), 459-484.

Hu, H.T. and Schnobrich, W.C. (1989), "Constitutive modeling of concrete by using nonassociated plasticity", *J. Mater. Civil Eng.*, **1**(4), 199-216.

Hu, H.T., Huang, C.S., Wu, M.H. and Wu, Y.M. (2003), "Nonlinear analysis of axially loaded concrete-filled tube columns with confinement effect", *J. Struct. Eng.*, **129**(10), 1323-1329.

Huang, C.S., Yeh, Y.K., Liu, G.Y., Hu, H.T., Tsai, K.C., Weng, Y.T., Wang, S.H. and Wu, M.H. (2002), "Axial load behavior of stiffened concrete-filled steel columns", *J. Struct. Eng.*, **128**(9), 1222-1230.

Janke, L., Czaderski, C., Ruth, J. and Motavalli, M. (2009), "Experiments on the residual load-bearing capacity of prestressed confined concrete columns", *Eng. Struct.*, **31**(10), 2247-2256.

Johansson, M. and Gylltoft, K. (2002), "Mechanical behavior of circular steel-concrete composite stub columns", *J. Struct. Eng.*, **128**(8), 1073-1081.

Krstulovic-Opara, N. and Thiedeman, P.D. (2000), "Active confinement of concrete members with self-stressing composites", *ACI Mater. J.*, **97**(3), 297-308.

Mander, J.B., Priestley, M.J.N. and Park, R. (1988), "Theoretical stress-strain model for confined concrete", *J. Struct. Eng.*, **114**(8), 1804-1826.

Martin, C.W. (1968), "Spirally prestressed concrete cylinders", *ACI J.*, **65**(10), 837-845.

Moghaddam, H., Samadi, M. and Pilakoutas, K. (2010), "Compressive behavior of concrete actively confined by metal strips; part B: Analysis", *Mater. Struct.*, **43**(10), 1383-1396.

Moghaddam, H., Samadi, M., Pilakoutas, K. and Mohebbi, S. (2010), "Axial compressive behavior of concrete actively confined by metal strips; part A: Experimental study", *Mater. Struct.*, **43**(10), 1369-1381.

Mokari, J. and Moghadam, A.S. (2008), "Experimental and theoretical study of reinforced concrete columns with poor confinement retrofitted by thermal post tension steel jacketing", *J. Appl. Sci.*, **8**(24), 4579-4586.

Mortazavi, A.A., Pilakoutas, K. and Son, K.S. (2003), "RC column strengthening by lateral pre-tensioning of FRP", *Constr. Build. Mater.*, **17**(6), 491-497.

Nematzadeh, M. and Naghipour, M. (2012), "Compressive strength and modulus of elasticity of freshly compressed concrete", *Constr. Build. Mater.*, **34**, 476-485.

Nematzadeh, M., Fazli, S., Naghipour, M. and Jalali, J. (2017c), "Experimental study on modulus of elasticity of steel tube-confined concrete stub columns with active and passive confinement", *Eng. Struct.*, **130**, 142-153.

Nematzadeh, M., Hajirasouliha, I., Haghinejad, A. and Naghipour, M. (2017a), "Compressive behaviour of circular steel tube-confined concrete stub columns with active and passive confinement", *Steel Compos. Struct.*, In press.

Nematzadeh, M., Naghipour, M., Jalali, J. and Salari, A. (2017b), "Experimental study and calculation of confinement relationships for prestressed steel tube-confined compressed concrete stub columns", *J. Civil Eng. Manage.*, In press.

Saenz, L.P. (1964), "Discussion of 'equation for the stress-strain curve of concrete' by P. Desayi, and S. Krishnan", *J. Am. Concrete Inst.*, **61**, 1229-1235.

Schneider, S.P. (1998), "Axially loaded concrete-filled steel tubes", *J. Struct. Eng.*, **124**(10), 1125-1138.

Shin, M. and Andrawes, B. (2010), "Experimental investigation of actively confined concrete using shape memory alloys", *Eng. Struct.*, **32**(3), 656-664.

Shinohara, Y. (2008), "Effect of transverse prestressing on shear behaviors of high-strength concrete columns", *Proceedings of the 14th World Conference on Earthquake Engineering*, Beijing, China, October.

Shraideh, M.S. and Aboutaha, R.S. (2013), "Analysis of steel-GFRP reinforced concrete circular columns", *Comput. Concrete*, **11**(4), 351-364.

Wang, W., Guo, Z. and Shi, Y. (2011), "Finite element analysis on behavior of the joint with steel tube confined concrete (STCC) column to reinforced concrete beam", *Adv. Mater. Res.*, **243**, 527-530.

Yu, Q., Tao, Z., Liu, W. and Chen, Z.B. (2010), "Analysis and calculations of steel tube confined concrete (STCC) stub columns", *J. Constr. Steel Res.*, **66**(1), 53-64.

CC